Unified Sufficient Conditions for Exact Convex Relaxation of Nonconvex Optimal Control Problems

Runqiu Yang, Member, IEEE
Weisong Wen, Member, IEEE
Peiwen Yang
Zichen Zhao
Fengtianyi Huang

***Abstract*— This paper focuses on achieving exact convex relaxation of optimal control problems characterized by nonconvex control constraints and convex state constraints. By employing the convex hull of the original nonconvex control constraint set, the constraints are relaxed, thereby transforming the original problem into a convex problem. The paper introduces two unified sufficient conditions to ensure the relaxation's exactness, guaranteeing that the solution derived from the relaxed problem remains globally optimal for the original nonconvex problem. Although one of the proposed sufficient conditions is abstract and nontrivial, we prove that it can be transformed into standard controllability, normality, and strong observability conditions proposed by the previous work about exact convex relaxation, if the control and state constraint sets have certain properties. Furthermore, approximation methods are developed to modify the cost function, control constraints, and system dynamics to ensure that the sufficient conditions are satisfied in certain scenarios. The results of this paper are applied to Mars landing problems, demonstrating that under glide-slope constraints, the exact convex can be realized.**

***Index Terms*— Optimal control, Convex relaxation, Convex optimization, Mars landing**

Notation

I_k	$k \times k$ identity matrix.
$(\cdot)^\top$	Transpose of a vector or matrix.
$a_{i:j}$	Subvector of the vector a from index i to j.
A_{ij}	(i,j)-entry of the matrix A.
$\mathrm{rank}A$	Rank of the matrix A.
$\|\cdot\|$	Euclidean norm.
$\|\cdot\|_{L^\infty}$	L^∞ norm.
$\mathrm{bd}\Omega$	Boundary of the set Ω.
$\mathrm{int}\Omega$	Interior of the set Ω.
$\mathrm{co}\Omega$	Convex hull of the set Ω.
$\mathrm{aff}\Omega$	Affine hull of the set Ω.
Ω'	Complement of the set Ω.
$\mathrm{aff}_0\Omega$	Subspace corresponding to the $\mathrm{aff}\Omega$, defined as $\mathrm{aff}_0\Omega = \mathrm{aff}\{x-y : x,\ y \in \Omega\}$.
$V^\perp$	Orthogonal complement of a vector subspace V.
$\mathrm{ri}C$	Relative interior of the convex set C.
$\mathrm{ext}C$	Extreme points of the convex set C.
$N_C(\bar{x})$	Normal cone to a convex set C at $\bar{x} \in C$, defined as $N_C(\bar{x}) = \{v : v^\top(x-\bar{x}) \leq 0,\ \forall\ x \in C\}$.
$B_\epsilon(x)$	Open ball centered at x with radius $\epsilon > 0$ in a metric space X.
$d(x,\Omega)$	Euclidean distance between a point x and a closed set Ω, defined as $d(x,\Omega) = \min_{y\in\Omega}\|x-y\|$.
a.e.	Almost everywhere.

I. Introduction

This paper investigates exact convex relaxation for optimal control problems (OCPs) governed by linear dynamical systems with general nonconvex control constraints and convex state constraints. The control constraints are defined by a nonconvex and compact set. Such nonconvex control constraints frequently arises in aerospace engineering, such as the planetary powered descent landing problems [1], [2], the rendezvous problems [3], the rocket landing problem [4], [5], the trajectory optimization problems of UAVs [6], etc.

The motivation for this work is to enable guidance based on real-time optimization. Historically, analytical guidance laws were widely used. These laws are among the simplest guidance approaches, which include the effective proportional navigation law and its variants for missiles [7], the Apollo lunar descent guidance [8] and the gravity-turn guidance [9] for planetary landers, and the iterative guidance for launch vehicles [10]. With significant advancements in onboard computing capabilities and the increasing complexity of tasks incorporating various constraints, the computational guidance [11], particularly the real-time optimization [2], [3], [12]–[15], has gained popularity. Real-time optimization demands the efficient and reliable solution of optimal control problems (OCPs) subject to diverse constraints. Since these OCPs are inherently nonconvex, they are commonly addressed using nonlinear programming (NLP) approaches [16]–[18]. However, NLP methods face inherent limitations: their convergence guarantees are restricted to local optima (and with a suitable initial guess), and even sometimes they fail to obtain feasible solutions. These challenges render NLP-based approaches inadequate for real-time resolution of nonconvex OCPs.

Runqiu Yang, Weisong Wen, and Peiwen Yang are with Department of Aeronautical and Aviation Engineering, The Hong Kong Polytechnic University, Hong Kong, China (e-mail: runqiu.yang@polyu.edu.hk; welson.wen@polyu.edu.hk; peiwen1.yang@connect.polyu.hk). Zichen Zhao is with School of Astronautics, Harbin Institute of Technology, Harbin 150001, China (e-mail: bitzhaozc@foxmail.com). Fengtianyi Huang is with School of Automation, Northwestern Polytechnical University, Xi'an 710129, China (e-mail: 1901385801@qq.com).

0018-9251 © IEEE

Given that convex optimization problems admit computationally efficient solutions via off-the-shelf interior-point methods with guaranteed polynomial-time convergence [19], [20], a promising strategy for nonconvex optimal control problems lies in their transformation into convex formulations. This is achieved through *exact convex relaxation* or *lossless convexification* technique, which preserves the global optimality of the original problem while enabling tractable computation. In the area of guidance, the exact convex relaxation was introduced in 2007 for the Mars powered descent landing [1]. Over the past decade, exact convex relaxation has attracted significant attention, with substantial research devoted to applying it to OCPs with various constraints [12], [21]–[30].

The existing works on exact convex relaxation have primarily focused on three cases related to the state constraints: 1) the state constraints are inactive, 2) the state constraints are active only at discrete points, and 3) the state constraints are consistently active (formulate the state constraints as equality constraints). In these scenarios, the achievement of exact convex relaxation mainly depends on two classes of conditions [12], [21]–[23], [25]. The first class comprises final-point conditions involving the gradient of the optimal trajectory's final state, while the second class is controllability-related conditions. The second class of conditions includes the system controllability [12], [21], strong controllability [22], strong observability of the adjoint system [23], [26], and the normality conditions [25]. However, the final-point condition is nontrivial and cannot generally be verified a priori due to its dependence on the optimal solution. To circumvent this limitation, the works [24], [28], [29] have developed alternative approaches that decompose the original nonconvex problem into either two or a sequence of convex subproblems. However, these existing conditions remain insufficient for more general cases where state constraints may be active over some subintervals, leaving an important gap in the theory of exact convex relaxation.

The root of this theoretical gap lies in the inapplicability of traditional proof techniques when general state constraints are present. The traditional approach for proving exactness relies on applying the maximum principle and deriving a contradiction to its non-triviality condition. However, the maximum principle under state constraints is structurally different, involving multipliers of bounded variation and a more complex non-triviality condition. This fundamental change prevents the standard proof method from guaranteeing a contradiction, rendering it infeasible for this broader and more challenging class of problems. A novel analytical approach is therefore required.

This paper first proposes two unified sufficient conditions to achieve the exact convex relaxation of nonconvex OCPs, applicable to both active and inactive state constraints. Then, based on the unified sufficient conditions, a novel proof technique is proposed to show the realization of the exact convex relaxation. Unlike the traditional proof that applies the maximum principle [31], [32] directly to the relaxed problem, we utilize the maximum principle under state constraints [33], [34] for a newly-constructed subproblem. While one of the proposed sufficient conditions is somewhat abstract, we demonstrate that it can be reduced to the previously used controllability-related conditions when control and state constraints have some certain forms. Furthermore, we develop systematic approximation techniques to reformulate the cost function, control constraints, and system dynamics. These modifications ensure guaranteed satisfaction of both sufficient conditions in well-defined operational scenarios while enabling arbitrarily small approximation errors. The practical utility of this framework is demonstrated through its application to the Mars landing problem. The proposed method makes exact convex relaxation achievable even for complex trajectories where the glide-slope constraint is active for a continuous period. This capability, not guaranteed by previous methods [1], [2], [35], enhances the reliability of real-time trajectory optimization for challenging landing scenarios. The principal contributions of this work are summarized as follows:

1) Establishment of two unified sufficient conditions for the realization of exact convex relaxation (cf. Condition 1-2 and Theorem 1).
2) Demonstration that Condition 2 can be reduced to the controllability-related conditions under specific control and state constraint set forms (cf. Theorem 2-3).
3) Introduction of approximation methods to ensure the satisfaction of sufficient conditions in specific scenarios (cf. Theorem 4-6).

The remainder of this paper is organized as follows. In Sec. II, we formally present the nonconvex OCP under investigation along with its convex relaxation. The unified sufficient conditions for the exact convex relaxation are presented in Sec. III. The transformation of one of the conditions is discussed in Sec. IV. Section V covers the approximation methods for satisfying the sufficient conditions. To validate our theoretical developments, Sec. VI presents a numerical case study of the Mars landing problem. Finally, this paper is concluded in Sec. VII.

II. Problem Formulation and Relaxation

This section formally presents the optimal control problem (OCP) under investigation and derives its convex relaxation.

A. Nonconvex Optimal Control Problem

In this paper, we consider the following nonconvex OCP.

Original Problem (OP)

$$\begin{aligned} \min \quad & \phi(x(t_f)) + \alpha \int_{t_0}^{t_f} a(t)^\top x(t) + b(t)^\top u(t) \mathrm{d}t \\ \text{s.t.} \quad & \dot{x}(t) = A(t)x(t) + B(t)u(t) + c(t) \\ & u(t) \in \mathcal{U} \\ & x(t) \in \mathcal{X} \\ & x(t_0) = x_0,\ x(t_f) \in \mathcal{E} \end{aligned} \tag{1}$$

where the state $x : [t_0, t_f] \to \mathbb{R}^n$ is absolutely continuous, the control $u : [t_0, t_f] \to \mathbb{R}^m$ is assumed to be piecewise continuous, $\phi : \mathbb{R}^n \to \mathbb{R}$ is convex, $A : [t_0, t_f] \to \mathbb{R}^{n\times n}$, $a : [t_0, t_f] \to \mathbb{R}^n$, $B : [t_0, t_f] \to \mathbb{R}^{n\times m}$, and $b : [t_0, t_f] \to \mathbb{R}^m$ are smooth, $c : \mathbb{R} \to \mathbb{R}^n$ is continuous, the control constraint set $\mathcal{U} \subset \mathbb{R}^m$ is nonconvex and compact, the state constraint set $\mathcal{X} \subset \mathbb{R}^n$ is convex and closed, t_0 and t_f denote the fixed initial and final time, respectively, x_0 is the fixed initial state, and the terminal set $\mathcal{E} \subset \mathbb{R}^n$ is closed and convex. In addition, we assume that both the feasible control constraint set $\mathcal{U}$ and state constraint set $\mathcal{X}$ can be expressed by a system of inequalities. The nonconvexity of the set $\mathcal{U}$ renders OP nonconvex, whose optimal value we denote by J_o^*.

REMARK 1 *This paper focuses exclusively on the fixed-final-time problem. In practice, when using convex optimization, free-final-time problems are typically transformed into fixed-final-time problems, which are then solved iteratively to get the optimal final time [1], [2]. Hence, it suffices to consider the exact convex relaxation of the fixed-final-time problems.*

B. Convex Relaxation

In this subsection, we first construct the relaxed problem (RP) with convex constraints. Subsequently, we review the conventional proof technique establishes the equivalence between the RP and OP solutions, while highlighting its limitations in handling the state-constrained OCP considered in this paper.

The OP is nonconvex due to the nonconvex constraints $u(t) \in \mathcal{U}$. To obtain a convex relaxation, we replace $\mathcal{U}$ with its convex hull $\mathrm{co}\mathcal{U}$, transforming the control constraints to $u(t) \in \mathrm{co}\mathcal{U}$. This convexification yields the following relaxed problem:

Relaxed Problem (RP)

$$\begin{aligned} \min \quad & \phi(x(t_f)) + \alpha \int_{t_0}^{t_f} a(t)^\top x(t) + b(t)^\top u(t) \mathrm{d}t \\ \text{s.t.} \quad & \dot{x}(t) = A(t)x(t) + B(t)u(t) + c(t) \\ & u(t) \in \mathrm{co}\mathcal{U} \\ & x(t) \in \mathcal{X} \\ & x(t_0) = x_0,\ x(t_f) \in \mathcal{E} \end{aligned} \tag{2}$$

Let (x^*, u^*) denote the global optimal solution of the RP, with J_r^* representing its optimal cost. We say the convex relaxation is exact when this solution is also globally optimal for the OP.

Next, we review the standard proof technique for the exact convex relaxation of the RP in the absence of state constraints. The maximum principle [31], [32] is typically applied to analyze the solution of the RP. In the maximum principle without state constraints, the non-triviality condition is: for each t, $(\lambda_0, \lambda(t)) \neq 0$ where λ is the costates, and the costate equations are linear and homogeneous with respect to (λ_0, λ), i.e.,

$$\begin{aligned} \dot{\lambda} &= -A(t)^\top \lambda - \alpha a(t)\lambda_0 \\ \dot{\lambda}_0 &= 0 \end{aligned} \tag{3}$$

Generally, the proof proceeds through three steps to establish $(\lambda_0, \lambda(t)) = 0$ which contradicts the non-triviality condition:

1) *Supposition*: Assume an interval or a set of positive measure where $u^*(t) \notin \mathcal{U}$;
2) *Deriving* $\lambda = 0$: Apply the pointwise maximum condition (or the stationary condition) and normality conditions [25], [26], [29] to the costate equations to derive $\lambda(t) = 0$ for each t;
3) *Deriving* $\lambda_0 = 0$: Given that $\lambda(t_f) = 0$, use transversality and final-point conditions to prove $\lambda_0 = 0$.

For cases where $\mathcal{X}$ is a submanifold (equality constraints only), the proof structure remains valid when replacing normality conditions with strong observability conditions [22], [26].

However, The introduction of general state constraints fundamentally alters this analysis. The maximum principle with state constraints significantly differs from that without state constraints.

For the maximum principle with state constraints proposed provided in [33], [34], the non-triviality condition is: $(\lambda_0, \lambda, \varphi) \neq 0$ holds in the norm of functions where φ is a normalized bounded variation related to the activeness of state constraints, and the costate equations include terms related to φ. If we follow the above steps, we encounter two main challenges. First, in Step 2, we may only derive $\lambda(t) = 0$ over the interval on which $u^*(t) \notin \mathcal{U}$. Second, even if we establish $(\lambda_0, \lambda) = 0$, it may still be insufficient to reach a contradiction, as we cannot further deduce $\varphi \neq 0$.

For the maximum principle with state constraints provided in [36], the non-triviality condition is: $(\lambda_0, \lambda(t), \nu(t), \eta_1, \eta_2, \dots) \neq 0$ for each t where ν is the multiplier related to state constraints and η_i are vectors related to each discontinuity of the costates, and the costate equations include terms related to ν. Likewise, if we use the standard steps, we encounter two main challenges. First, in Step 2, we may only derive $\lambda(t) = 0$ over the interval on which $u^*(t) \notin \mathcal{U}$. Second, even if we establish $(\lambda_0, \lambda(t), \nu(t)) = 0$ on some t, it may still be insufficient to reach a contradiction, as we cannot further deduce $(\eta_1, \eta_2, \dots) \neq 0$. In summary, the presence of state constraints renders the traditional proof technique infeasible.

In this paper, we will handle this issue and propose a novel proof procedure with the unified sufficient conditions presented in the following section to show the

realization of the exact convex relaxation for the OCP with state constraints.

III. Sufficient Conditions

In this section, we propose two unified sufficient conditions, and provide a novel proof technique of exact convex relaxation for the state-constrained optimal control problem.

The first sufficient condition requires the cost function to have an integral term as follows

CONDITION 1 *The parameter α in the cost function is nonzero.*

Before presenting the second sufficient condition, we first characterize the geometric structure of the relaxation gap $\mathrm{co}\mathcal{U}\setminus\mathcal{U}$ and the state constraint set $\mathcal{X}$. Any convex set can be expressed as the disjoint union of relative interiors of its non-empty faces[1] (cf. Theorem 18.2 of [37]). This yields the covering $\mathrm{co}\mathcal{U}\setminus\mathcal{U}\subset\cup_\gamma \mathrm{ri}\mathcal{M}_\gamma$, where each $\mathcal{M}_\gamma$ is a face of $\mathrm{co}\mathcal{U}$ with $\mathrm{ri}\mathcal{M}_\gamma\cap(\mathrm{co}\mathcal{U}\setminus\mathcal{U})\neq\emptyset$. While this union may be infinite and even uncountable, we construct a finite partition $\{\Gamma_i\}_{i=1}^{k_u}$, where each Γ_i is a finite or infinite union of $\{\mathrm{ri}\mathcal{M}_\gamma\}$, and $\{\Gamma_i\}_{i=1}^{k_u}$ are mutually disjoint. Thus, $\mathrm{co}\mathcal{U}\setminus\mathcal{U}$ can also be expressed by

$$\mathrm{co}\mathcal{U}\setminus\mathcal{U}\subset\cup_{i=1}^{k_u}\Gamma_i \tag{4}$$

Similarly, for the convex set $\mathcal{X}$, we can also define a finite collection $\{\Xi_j\}_{j=0}^{k_x}$ such that

$$\mathcal{X}=\cup_{j=0}^{k_x}\Xi_j,\ \Xi_0=\mathrm{int}\mathcal{X} \tag{5}$$

REMARK 2 *The partitions of $\mathrm{co}\mathcal{U}\setminus\mathcal{U}$ and $\mathcal{X}$ can be constructed straightforwardly in practice. For instance, since the control and state constraint sets can be expressed by a system of inequalities, suppose that the sets $\mathcal{U}$, $\mathrm{co}\mathcal{U}$, and $\mathcal{X}$ have the forms as follows*

$$\mathcal{U}=\{u: r(u)=0,\ h_i(u)\le 0,\ i=1,\dots,l\} \tag{6}$$
$$\mathrm{co}\mathcal{U}=\{u: r(u)\le 0,\ h_i(u)\le 0,\ i=1,\dots,l\} \tag{7}$$
$$\mathcal{X}=\{x: g_j(u)\le 0,\ j=1,\dots,s\} \tag{8}$$

The exact convex relaxation requires that the inequality constraint $r(u(t))\le 0$ remains consistently active. To prove this, it is necessary to verify whether $r(u(t))\le 0$ is active under various combinations where some of the constraints $h_i(u(t))\le 0$ are active while others are inactive. Thus, the collection can be constructed based on these combinations, i.e.,

$$\Gamma_i=\{u: r(u)<0,\ h_I(u)=0,\ h_{I'}(u)<0\} \tag{9}$$

where $I\subset\{1,\dots,l\}$. Likewise, based on the form of state constraint set (8), the collection can be constructed based on the combinations, i.e.,

$$\Xi_j=\{x: g_J(u)=0,\ g_{J'}(u)<0\} \tag{10}$$

where $J\subset\{1,\dots,s\}$.

[1]A face of a convex set Ω is a convex subset $\Omega'\subset\Omega$ containing all line segments that pass through its relative interior [37].

Based on the partitions $\{\Gamma_i\}_{i=1}^{k_u}$ and $\{\Xi_j\}_{j=0}^{k_x}$, the second sufficient condition is as follows

CONDITION 2 *For each pair (Γ_i,Ξ_j) and for each subinterval $[t_1,t_2]\subset[t_0,t_f]$ on which $x^*(t)\in\Xi_j$, we consider the linear input-output system:*

$$\begin{aligned}\dot p(t)&=-\hat A(t)^\top p(t)-\hat A(t)^\top\psi(t)\\ y(t)&=\hat B(t)^\top(p(t)+\psi(t))\end{aligned} \tag{11}$$

where $p:[t_1,t_2]\to\mathbb{R}^{n+1}$ is the absolutely continuous state, $y:[t_1,t_2]\to\mathbb{R}^m$ is the output,

$$\hat A=\begin{bmatrix}A(t) & 0\\ \alpha a(t)^\top & 0\end{bmatrix},\ \hat B=\begin{bmatrix}B(t)\\ \alpha b(t)^\top\end{bmatrix} \tag{12}$$

The input $\psi:[t_1,t_2]\to\mathbb{R}^{n+1}$ is a normalized function of bounded variation defined through the Lebesgue-Stieltjes integral:

$$\psi(t)=\int_{[t_1,t]}\nu(\tau)\mathrm{d}\mu(\tau) \tag{13}$$

$$\begin{aligned}&\nu_{1:n}(t)\in N_{\mathcal{X}}(x^*(t))\cap B_1(0)\\ &\nu_{n+1}(t)=0\end{aligned}\quad \mu-a.e.\ [t_1,t_2] \tag{14}$$

where μ is a Radon measure on $[t_1,t_2]$ and $\nu:[t_1,t_2]\to\mathbb{R}^{n+1}$ is a Borel measurable function. For each $t\in[t_1,t_2]$ the output $y(t)$ orthogonal to $\mathrm{aff}_0\mathcal{M}$ of a face with $\mathrm{ri}\mathcal{M}\subset\Gamma_i$ implies that the pair (p,ψ) is identically zero.

While Condition 2 may appear abstract at first glance, it actually serves as a natural generalization of the well-known controllability-related conditions. In the following section, we will demonstrate that when the constraint sets $\mathcal{X}$ and $\mathcal{U}$ possess certain specific properties, the classical controllability-related conditions are sufficient to guarantee Condition 2.

Furthermore, we establish the following fundamental result connecting the RP to the OP:

THEOREM 1 *Under Condition 1-2, any solution (x^*,u^*) of the RP is also an optimal solution of the OP.*

Proof:
We proceed by contradiction. Assume there exists a subset $E\subset[t_0,t_f]$ of positive measure on which $u^*(t)\notin\mathcal{U}$. By construction, $u^*\in\mathrm{co}\mathcal{U}\setminus\mathcal{U}$. From Eq. (4), $\mathrm{co}\mathcal{U}\setminus\mathcal{U}$ can be covered by finitely many disjoint $\{\Gamma_i\}_{i=1}^{k_u}$. Given that u^* is piecewise continuous, there exists an interval $I\subset E$ and a certain Γ_i such that $u^*(t)\in\Gamma_i$. In addition, since x is continuous, there exists an interval $[t_1,t_2]\subset I\subset E$ and a certain Ξ_j such that $x^*(t)\in\Xi_j$. Given that $\alpha\neq 0$ (Condition 1), we then construct a subproblem on this interval as follows

$$\begin{aligned}\min\quad & \alpha\int_{t_1}^{t_2}a(t)^\top x(t)+b(t)^\top u(t)\mathrm{d}t\\ \text{s.t.}\quad & \dot x(t)=A(t)x(t)+B(t)u(t)+c(t)\\ & u(t)\in\mathrm{co}\mathcal{U}\\ & x(t)\in\mathcal{X}\\ & x(t_1)=x^*(t_1),\ x(t_f)=x^*(t_2)\end{aligned} \tag{15}$$

First, we show that the solution (x^*, u^*) on $[t_1, t_2]$ is optimal to the subproblem by contradiction. Suppose that (x^+, u^+) solves the subproblem with

$$\begin{aligned}&\alpha \int_{t_1}^{t_2} a(t)^\top x^+(t) + b(t)^\top u^+(t)\mathrm{d}t \\ &< \alpha \int_{t_1}^{t_2} a(t)^\top x^*(t) + b(t)^\top u^*(t)\mathrm{d}t\end{aligned} \tag{16}$$

Then, we construct a solution pair $(\bar{x}, \bar{u})$ as follows

$$\begin{aligned}\bar{x}(t) &= \begin{cases} x^*(t) & [t_0, t_f] \setminus [t_1, t_2] \\ x^+(t) & (t_1, t_2) \end{cases} \\ \bar{u}(t) &= \begin{cases} u^*(t) & [t_0, t_f] \setminus [t_1, t_2] \\ u^+(t) & (t_1, t_2) \end{cases}\end{aligned} \tag{17}$$

Obviously, the solution $(\bar{x}, \bar{u})$ is a feasible solution of the RP, and its cost satisfies

$$\begin{aligned}&\phi(\bar{x}(t_f)) + \alpha \int_{t_0}^{t_f} a(t)^\top \bar{x}(t) + b(t)^\top \bar{u}(t)\mathrm{d}t \\ =&\phi(x^*(t_f)) + \alpha \int_{[t_0,t_1]\cup[t_2,t_f]} a(t)^\top x^*(t) + b(t)^\top u^*(t)\mathrm{d}t \\ &+\alpha \int_{t_1}^{t_2} a(t)^\top x^+(t) + b(t)^\top u^+(t)\mathrm{d}t \\ <&\phi(x^*(t_f)) + \alpha \int_{t_0}^{t_f} a(t)^\top x^*(t) + b(t)^\top u^*(t)\mathrm{d}t\end{aligned} \tag{18}$$

where the last inequality follows from Eq. (16). This contradicts the optimality of (x^*, u^*) for the RP.

Since (x^*, u^*) is optimal to the subproblem, it must satisfy the first-order optimality conditions. According to the maximum principle with state constraints [33], [34], there exist $\lambda_0 \in \{0, 1\}$, an absolutely continuous function $\lambda : [t_1, t_2] \to \mathbb{R}^n$, and $\varphi : [t_1, t_2] \to \mathbb{R}^n$ of normalized bounded variation defined by

$$\varphi(t) = \int_{[t_1,t]} \upsilon(\tau)\mathrm{d}\mu(\tau) \tag{19}$$

$$\upsilon(t) \in N_{\mathcal{X}}(x^*(t)) \cap B_1(0),\ \mu - \text{a.e. } [t_1, t_2] \tag{20}$$

not vanishing simultaneously such that
(i) costate equations:

$$\dot{\lambda}(t) = -A(t)^\top \lambda(t) - A(t)^\top \varphi(t) + \lambda_0 \alpha a(t) \tag{21}$$

(ii) pointwise maximum condition:

$$u^*(t) = \arg\max_{z \in \mathrm{co}\mathcal{U}} \left[(q(t) + \varphi(t))^\top B(t) + \alpha b(t)^\top\right] z \tag{22}$$

Define $p := [\lambda^\top \ \lambda_0]^\top$ and $\psi := [\varphi^\top \ 0]^\top$. It follows from Eq. (11) that the costate equations and the pointwise maximum condition become

$$\dot{p}(t) = -\hat{A}(t)^\top p(t) - \hat{A}(t)^\top \psi(t) \tag{23}$$

$$u^*(t) = \arg\max_{z \in \mathrm{co}\mathcal{U}} y(t)^\top z \tag{24}$$

Since $u^*(t) \in \Gamma_i$, for each $t \in [t_1, t_2]$ $u^*(t)$ lies on $\mathrm{ri}\mathcal{M}$ of a face with $\mathrm{ri}\mathcal{M} \in \Gamma_i$. Based on the pointwise maximum condition (24), the supremum of the convex function $y(t)^\top z$ attains its supremum relative to the face $\mathcal{M}$ at a point of $\mathrm{ri}\mathcal{M}$, so $y(t)^\top z$ is constant through $\mathcal{M}$ (cf. Theorem 32.1 of [37]). Therefore, $y(t)^\top z = 0$ for each $z \in \{z_1 - z_2 : z_1, z_2 \in \mathcal{M}\}$. Given that each point of $\mathrm{aff}_0\mathcal{M}$ is a linear combination of the points in $\{z_1 - z_2 : z_1, z_2 \in \mathcal{M}\}$, $y(t)^\top z = 0$ also holds on $\mathrm{aff}_0\mathcal{M}$, which implies that $y(t)$ is orthogonal to $\mathrm{aff}_0\mathcal{M}$. It follows from Condition 2 that $(p, \psi) = 0$, which implies that λ_0, q, and φ vanish simultaneously. This is a contradiction. Therefore, $u^*(t) \in \mathcal{U}$ a.e. on $[t_0, t_f]$.

Since $u^*(t) \in \mathcal{U}$ a.e. on $[t_0, t_f]$, (x^*, u^*) is feasible to the OP, which implies $J_r^* \geq J_o^*$. The RP is a relaxation of the OP, so $J_r^* \leq J_o^*$. Therefore, $J_r^* = J_o^*$, which means (x^*, u^*) is an optimal solution of the OP. ■

REMARK 3 *The proof methodology developed for Theorem 1 represents a significant departure from conventional approaches reviewed in Sec. II. Instead of directly applying the maximum principle to the RP, our approach focuses on constructing a local subproblem based on Condition 1 and leveraging Condition 2 to reach a contradiction as the maximum principle is applied to the subproblem.*

When Condition 1-2 are satisfied, the exact convex relaxation can be achieved. However, Condition 1-2 are nontrivial, and especially Condition 2 may not be verifiable a priori. In the next section, we will discuss how to transform this condition into some more straightforward conditions if the sets $\mathcal{X}$ and $\mathcal{U}$ have some certain properties.

IV. Condition Transformation

In this section, by confining the forms of $\mathcal{U}$ and $\mathcal{X}$, we show that Condition 2 can reduce to various controllability-related conditions. The discussion will be developed based on two different classes of subintervals $[t_1, t_2] \subset [t_0, t_f]$, i.e., the subintervals on which $x^*(t) \in \mathrm{int}\mathcal{X} = \Xi_0$ and $x^* \in \mathrm{bd}\mathcal{X} = \cup_{j=1}^{k_x} \Xi_j$.

In addition, we focus on two specific types of $\mathcal{U}$:

1) Type 1: $\mathcal{U}$ satisfies $\mathrm{bd}(\mathrm{co}\mathcal{U}) \subset \mathcal{U}$, such as an annular set in $\mathbb{R}^2$ or a spherical set in $\mathbb{R}^3$;
2) Type 2: there are finitely many of faces $\{\mathcal{M}_i\}_{i=1}^{k_u}$ in $\mathrm{co}\mathcal{U}$ such that $\mathrm{co}\mathcal{U} \setminus \mathcal{U} \subset \cup_{i=1}^{k_u} \mathrm{ri}\mathcal{M}_i$, such as a finite discrete set or a star-shaped set.

For Type 1, it is evident that $\mathrm{co}\mathcal{U} \setminus \mathcal{U}$ is contained in the relative interior of $\mathrm{co}\mathcal{U}$. For Type 2, $\mathrm{co}\mathcal{U} \setminus \mathcal{U}$ is contained in the relative interiors of finitely many faces. Thus, for both types, we construct the collection $\{\Gamma_i\}_{i=1}^{k_u}$ [cf. Eq. (4)] as $\{\mathrm{ri}\mathcal{M}_i\}_{i=1}^{k_u}$.

A. Inactive State Constraints

Since state constraints are inactive on the subinterval $[t_1, t_2]$, i.e., $x^*(t) \in \mathrm{int}\mathcal{X}$, Eq. (14) implies that $\nu(t) = 0$, μ-a.e. on $[t_1, t_2]$, and consequently $\psi = 0$. Therefore, the linear system (11) reduces to

$$\begin{aligned}\dot{p}(t) &= -\hat{A}(t)^\top p(t) \\ y(t) &= \hat{B}(t)^\top p(t)\end{aligned} \tag{25}$$

First, for $\mathcal{U}$ of Type 1, we have

LEMMA 1 *Suppose $x^*(t) \in \text{int}\mathcal{X}$ on $[t_1, t_2]$ and $\mathcal{U}$ belongs to Type 1. If $y(t)$ orthogonal to $\text{aff}_0(\text{co}\mathcal{U})$ for each $t \in [t_1, t_2]$, then $(p, \psi) = 0$ provided that $(\hat{A}, \hat{B})$ is controllable.*

Proof:
From $x^*(t) \in \text{int}\mathcal{X}$, we have $\psi = 0$. Since $y(t)$ is orthogonal to $\text{aff}_0(\text{co}\mathcal{U}) = \mathbb{R}^m$ for each $t \in [t_1, t_2]$, the output of the system (25) is zero. Due to the controllability of $(\hat{A}, \hat{B})$, $(-\hat{A}^\top, \hat{B}^\top)$ is observable thus resulting in $p = 0$. ■

Second, for $\mathcal{U}$ of Type 2, we can construct a finite collection $\mathcal{W}$ of nonzero test vectors, such that $\mathcal{W} \cap \text{aff}_0\mathcal{M}_i \neq \emptyset$ holds for each face $\mathcal{M}_i$. Based on the set $\mathcal{W}$, we give the definition of the normality as follows

DEFINITION 1 ([25], [28], [29]) *The system $(\hat{A}, \hat{B})$ with the set $\mathcal{W}$, denoted by $(\hat{A}, \hat{B}, \mathcal{W})$, is said to be normal if for each $w \in \mathcal{W}$, the matrix*

$$W(t) = [\hat{B}_1(t)w \ \hat{B}_2(t)w \ \cdots \ \hat{B}_{n+1}(t)w] \tag{26}$$

is nonsingular a.e. on $[t_1, t_2]$, where the matrix-valued functions $\hat{B}_i(t)$ are defined recursively by:

$$\begin{aligned} &\hat{B}_1(t) = \hat{B}(t) \\ &\hat{B}_i(t) = -\hat{A}(t)\hat{B}_{i-1}(t) + \dot{\hat{B}}_{i-1}(t), \ i = 2, \ldots, n+1 \end{aligned} \tag{27}$$

With the definition of the normality, we have

LEMMA 2 *Suppose $x^*(t) \in \text{int}\mathcal{X}$ on $[t_1, t_2]$ and $\mathcal{U}$ belongs to Type 2. For each $\mathcal{M}_i$, if $y(t)$ orthogonal to $\text{aff}_0\mathcal{M}_i$ for each $t \in [t_1, t_2]$, then $(p, \psi) = 0$ provided that $(\hat{A}, \hat{B}, \mathcal{W})$ is normal.*

Proof:
From $x^*(t) \in \text{int}\mathcal{X}$, we have $\psi = 0$. Since for each $t \in [t_1, t_2]$, $y(t)$ is orthogonal to a specific $\text{aff}_0\mathcal{M}_i$. By the form of $\mathcal{W}$, there exist $w \in \mathcal{W}$ such that $w \in \text{aff}_0\mathcal{M}_i$. Hence, on $[t_1, t_2]$, $w^\top\hat{B}(t)^\top p(t) = 0$. Utilizing Eq. (27) and differentiating both sides of the equation $w^\top\hat{B}(t)^\top p(t) = 0$ sequentially n times yields

$$p(t)^\top[\hat{B}_1(t)w \ \hat{B}_2(t)w \ \cdots \ \hat{B}_{n+1}(t)w] = 0 \tag{28}$$

This implies that $W(t)^\top p(t) = 0$. Since $W(t)$ is nonsingular a.e. on $[t_1, t_2]$ and p is continuous, $p = 0$. ■

B. Active State Constraints

On a subinterval where state constraints are active, the situation becomes significantly more complex due to the existence of the normalized bounded variation ψ. The complexity arises because ψ can be highly irregular and have an infinite number of jumps [38]. To ensure that ψ has a specific degree of smoothness, we impose the following regularity conditions [33]

ASSUMPTION 1 ([33]) *(i) The set $\mathcal{X}$ can be expressed by $\mathcal{X} = \cap_{j=1}^k \mathcal{X}_j$ for some closed sets $\mathcal{X}_j$ with $\text{bd}\mathcal{X}_j$ being a $C^{1,1}$-manifold with a positive reach[2]. Additionally, 0 does not belong to $\text{co}\{n_j(x) : j \in \mathcal{J}(x)\}$ where $\mathcal{J}(x) = \{j \in \{1, \ldots, k\} : x \in \text{bd}\mathcal{X}_j\}$ is the active index set at x and $n_j(x)$ is the outward unit normal to $\mathcal{X}_j$ at x;*

(ii) The optimal Hamiltonian

$$\mathcal{H}(t, x^*(t), p) = \sup_{z \in \mathcal{U}}[p^\top f(t, x^*(t), z) - l(t, x^*(t), z)]p^\top \tag{29}$$

where $t \in [t_1, t_2]$, f represents the right side of the system and l is the integrand of the cost function in the RP, is continuous, $\partial_p\mathcal{H}$ is locally Lipschitz, and $\partial_p\mathcal{H}$ satisfies a coercivity condition (details can be found in [33]).

In Assumption 1, condition (i) pertains to state constraints and can be readily verified, whereas condition (ii) is more challenging to confirm and is assumed to hold throughout this subsection. If Assumption 1 is satisfied, ψ is absolutely continuous on (t_1, t_2) [33], which implies that $\dot{\psi}$ exists a.e. on (t_1, t_2). From Eq. (13), we have $\dot{\psi}(t) = \nu(t)$. Defining $q := p + \psi$, Eq. (14) implies that the system (11) can be transformed into

$$\begin{aligned} &\dot{q}(t) \in -\hat{A}(t)^\top q(t) + \{[\nu^\top \ 0]^\top : \nu \in N_{\mathcal{X}}(x^*(t))\} \\ &y(t) = \hat{B}(t)^\top q(t) \end{aligned} \tag{30}$$

We focus on n-dimensional linear state constraints in this subsection

$$\mathcal{X} = \{x : Gx \leq g\} \tag{31}$$

where $G \in \mathbb{R}^{s \times n}$. The set can be written as

$$\mathcal{X} = \cap_{j=1}^s \mathcal{X}_j = \cap_{j=1}^s \{x : G_j x \leq g_j\} \tag{32}$$

where G_j is the j-th row of G and g_j is the j-th element of g. The set $\mathcal{X}_j$ is a closed half-space, and its boundary is a hyperplane, which implies that $\text{bd}\mathcal{X}_i$ is a smooth manifold with infinite reach. At any point x, the outward unit normal vector to $\mathcal{X}_i$ is simply $n_j(x) = G_j$. Then, we show that for each x, there do not exist $j_1, j_2 \in \mathcal{J}(x)$ such that $G_{j_1} = -G_{j_2}$. Otherwise, this would imply that $G_{j,1}x = g_{j,1}$ and $G_{j,2}x = g_{j,2}$, which lead to $g_{j,1} = -g_{j,2}$. Therefore, $\{x : G_{j,1}x \leq g_{j,1}\}$ and $\{x : G_{j,1}x \geq g_{j,1}\}$ exist in the set $\mathcal{X}$ at the same time. This contradicts the fact that $\mathcal{X}$ is n-dimensional. Therefore, $G_{j_1} \neq -G_{j_2}$ for any $j_1, j_2 \in \mathcal{J}(x)$, which implies that $0 \notin \text{co}\{n_j(x) : j \in \mathcal{J}(x)\}$. Thus, condition (i) of Assumption 1 is satisfied. Furthermore, each Ξ_j corresponds to $\{x : G_J x = g_J, \ Gg_{J'}x < g_{J'}\}$ for some $J \subset \{1, \ldots, s\}$. If we define $D_j = G_J$, then for $x^*(t) \in \Xi_j$, there exists a measurable function θ such that $\dot{\psi} = \hat{D}_j\theta$ where $\hat{D}_j = [D_j \ 0]^\top$ and Eq. (30) becomes

$$\begin{aligned} &\dot{q}(t) = -\hat{A}(t)^\top q(t) + \hat{D}_j\theta(t) \\ &y(t) = \hat{B}(t)^\top q(t) \end{aligned} \tag{33}$$

First, for $\mathcal{U}$ of Type 1, we have

[2]The reach τ_M of a manifold $M \subset \mathbb{R}^n$ is the largest $r \geq 0$ such that every point $y \in \mathbb{R}^n$ with $d(y, M) < r$ has a unique closest point projection onto M [39]. Specifically, if $\tau_M = \infty$, then every point in $\mathbb{R}^n$ has a unique projection onto M.

LEMMA 3 *Suppose that $x^*(t) \in \Xi_j$ on $[t_1, t_2]$ and $\mathcal{U}$ belongs to Type 1. Under Assumption 1, if $y(t)$ orthogonal to $\mathrm{aff}_0(\mathrm{co}\mathcal{U})$ for each $t \in [t_1, t_2]$, then $(p, \psi) = 0$ provided that $(-\hat{A}^\top, \hat{D}_j, \hat{B}^\top, 0)$ is strongly observable (the definition of strong observability can be found in Appendix).*

Proof:
Since for each $t \in [t_1, t_2]$, the output $y(t)$ is orthogonal to $\mathrm{aff}_0(\mathrm{co}\mathcal{U}) = \mathbb{R}^m$, the output of the system (33) is zero. The strong observability of $(-\hat{A}^\top, \hat{D}_j, \hat{B}^\top, 0)$ implies that q is identically zero, leading to $\dot{\psi} = \hat{D}_j\theta$ also being identically zero [cf. Eq. (33)]. Based on the integral $\psi(t) = \psi(t_1) + \int_{t_1}^{t} \dot{\psi}(\tau)\mathrm{d}\tau$, we get ψ is identically zero (the value of a normalized bounded variation at the initial point is zero [33]). Therefore, $p = q - \psi$ is also identically zero, implying $(p, \psi) = 0$. ■

Second, for $\mathcal{U}$ of Type 2, the orthogonal complement $(\mathrm{aff}_0\mathcal{M}_i)^\perp$ of each face $\mathcal{M}_i$ is a subspace of $\mathbb{R}^m$. We use r_i to denote the dimension of this subspace. For each subspace $(\mathrm{aff}_0\mathcal{M}_i)^\perp$, a set of basis is defined by a matrix $C_i \in \mathbb{R}^{m\times r_i}$, which indicates that $z \in (\mathrm{aff}_0\mathcal{M}_i)^\perp$ can be expressed by $z = C_i v$ for some $v \in \mathbb{R}^{r_i}$. Then, if we define $\hat{D}_j^0 := [\hat{D}_j\ 0]$ and ${}^0C_i := [0\ C_i]$, we have

LEMMA 4 *Suppose that $x^*(t) \in \Xi_j$ on $[t_1, t_2]$ and $\mathcal{U}$ belongs to Type 2. Under Assumption 1, for each $\mathcal{M}_i$, if $y(t)$ orthogonal to $\mathrm{aff}_0\mathcal{M}_i$ for each $t \in [t_1, t_2]$, then $(p, \psi) = 0$ provided that $(-\hat{A}^\top, \hat{D}_j^0, \hat{B}^\top, -{}^0C_i)$ is strongly observable for each $i = 1, \ldots, k_u$.*

Proof:
Since for each $t \in [t_1, t_2]$, the output $y(t)$ remains orthogonal to a certain $\mathrm{aff}_0\mathcal{M}_i$. This implies that there exists a measurable function $v : [t_1, t_2] \to \mathbb{R}^{r_i}$ such that $y(t) = C_i v(t)$. Therefore, the system (33) admits the following reformulation

$$\begin{aligned} \dot{q}(t) &= -\hat{A}(t)^\top q(t) + [\hat{D}_j\ 0]\begin{bmatrix}\theta(t)\\ v(t)\end{bmatrix} \\ 0 &= \hat{B}(t)^\top q(t) - [0\ C_i]\begin{bmatrix}\theta(t)\\ v(t)\end{bmatrix} \end{aligned} \tag{34}$$

The strong observability of $(-\hat{A}^\top, \hat{D}_j^0, \hat{B}^\top, -{}^0C_i)$ implies that q is identically zero, so $\dot{\psi} = \hat{D}_j\theta$ is also identically zero [cf. Eq. (34)]. Based on the integral $\psi(t) = \psi(t_1) + \int_{t_1}^{t} \dot{\psi}(\tau)\mathrm{d}\tau$, we get ψ is identically zero. Therefore, $p = q - \psi$ is also identically zero, implying $(p, \psi) = 0$. ■

For the control constraint set of Type 1 and the linear state constraints, we can directly derive the following theorem based on Lemma 1 and 3

THEOREM 2 *Suppose that $\mathcal{U}$ belongs to Type 1. Under Assumption 1, Condition 2 holds if $(\hat{A}, \hat{B})$ is controllable and $(-\hat{A}^\top, \hat{D}_j, \hat{B}^\top, 0)$ is strongly observable for each $j = 1, \ldots, k_x$.*

For the control constraint set of Type 2 and the linear state constraints, we can directly derive the following theorem based on Lemma 2 and 4

THEOREM 3 *Suppose that $\mathcal{U}$ belongs to Type 2. Under Assumption 1, Condition 2 holds if $(\hat{A}, \hat{B}, \mathcal{W})$ is normal and $(-\hat{A}^\top, \hat{D}_j^0, \hat{B}^\top, -{}^0C_i)$ is strongly observable for each $i = 1, \ldots, k_u$ and $j = 1, \ldots, k_x$.*

In sum, if the control and state constraint sets have specific forms, Condition 2 can be reduced to different controllability, normality, and strong observability conditions.

REMARK 4 *If the state constraints are convex but nonlinear, we can utilize the polyhedral approximation methods of convex sets to transform the original convex state constraints into linear ones [40], [41]. Therefore, the results in Theorem 2 and 3 can also be used for the cases with general convex state constraints.*

V. Condition Approximation

While Condition 1-2 serve as fundamental requirements for exact convex relaxation, practical scenarios may arise where these conditions are not inherently satisfied. To address such cases, this section develops systematic approximation techniques that enable the fulfillment of these conditions in specific operational contexts. Crucially, these approximation methods maintain theoretical rigor by ensuring that the introduced errors can be reduced to negligible levels through appropriate parameter selection.

A. Cost Function Approximation

If the cost function of the OP is in Mayer form ($\alpha = 0$), we can construct a regularized version by introducing a small perturbation parameter $\alpha > 0$. This perturbation incorporates an integral term through selected vectors a and b, yielding the modified cost function

$$J^\alpha = \phi(x(t_f)) + \alpha \int_{t_0}^{t_f} a^\top x(t) + b^\top u(t)\mathrm{d}t \tag{35}$$

Note that the original cost function is simply $J^0 = \phi(x(t_f))$.

Next, we prove that the approximation error (i.e., the increase in the optimal cost) introduced by adding an integral term to the cost function can be made arbitrarily small. Let (x_*^α, u_*^α) denote the optimal solution of perturbed problem, and define $\phi_*^\alpha := \phi(x_*^\alpha(t_f))$. For the original Mayer problem (OP), the optimal cost is denoted by J_*^0.

THEOREM 4 *For any desired accuracy $\varepsilon > 0$, there exists a perturbation parameter $\alpha > 0$ such that ϕ_*^α satisfies that $0 \le \phi_*^\alpha - J_*^0 \le \varepsilon$.*

Proof:

First, we consider the constrained linear system

$$\begin{aligned} &\dot{x}(t) = A(t)x(t) + B(t)u(t) + c(t) \\ &\dot{\xi}(t) = a^\top x(t) + b^\top u(t) \\ &u(t) \in \mathcal{U} \\ &x(t_0) = x_0,\ \xi(t_0) = 0 \end{aligned} \tag{36}$$

where it is evident that $\xi(t_f) = \int_{t_0}^{t_f} a^\top x(t) + b^\top u(t)\mathrm{d}t$. It follows from Theorem 1A on p.164 of [42] and compactness of $\mathcal{U}$ that the attainable set $\mathcal{R}(t_f)$, i.e., the set of all endpoints $[x(t_f)^\top\ \xi(t_f)]^\top$ in $\mathbb{R}^{n+1}$, is compact. If the constraints $x(t) \in \mathcal{X}$ and $x(t_f) \in \mathcal{E}$ are considered in system (36), the corresponding attainable set will be a subset of $\mathcal{R}(t_f)$ and remains bounded. Thus, there exists a $\zeta \geq 0$ such that $|\xi(t_f)| \leq \zeta$.

If $\zeta = 0$, it indicates that the integral term in the perturbed cost function (35) is identically zero, implying $J^\alpha = J^0$, and hence $\phi_*^\alpha = J_*^0$. If $\zeta > 0$, we set $\alpha = \varepsilon/(2\zeta)$. It is clear that the solution (x_*^α, u_*^α) of the OP with the perturbed cost function is feasible to the OP with the original one. Thus, $J_*^0 \leq \phi_*^\alpha$, i.e., $\phi_*^\alpha - J_*^0 \geq 0$. Additionally, the solution (x_*^0, u_*^0) of the OP with the original cost function is also feasible to the OP with the perturbed one, which implies

$$\phi_*^\alpha + \alpha\xi_*^\alpha(t_f) \leq \phi(x_*^0(t_f)) + \alpha\xi_*^0(t_f) \tag{37}$$

where $\xi_*^i(t_f) = \int_{t_0}^{t_f} a^\top x_*^i(t) + b^\top u_*^i(t)\mathrm{d}t$, $i = \alpha, 0$. Since $J_*^0 = \phi(x^*(t_f))$, Eq. (37) can yield

$$\phi_*^\alpha - J_*^0 \leq \alpha\left[\xi_*^0(t_f) - \xi_*^\alpha(t_f)\right] \leq \alpha\left[\zeta - (-\zeta)\right] = \varepsilon \tag{38}$$

where the second inequality follows from $|\xi(t_f)| \leq \zeta$ and the first equality follows from $\alpha = \varepsilon/(2\zeta)$. ■

REMARK 5 *While Theorem 4 guarantees that the approximation error can be made arbitrarily small from a theoretical standpoint, the practical choice of α involves a numerical trade-off. It must be large enough to be numerically significant for the solver but small enough to ensure the perturbed solution remains close to the original. An excessively small α could lead to ill-conditioning, where the integral term has a negligible effect on the optimization compared to solver tolerances.*

In sum, for a Mayer problem, introducing an integral term into the cost function ensures the satisfaction of Condition 1. According to Theorem 4, the loss of the optimality resulting from the approximation can be made arbitrarily small.

B. Control Set and System Approximation

Condition 2 is nontrivial, making it generally difficult to directly satisfy it for an OP. In this subsection, we provide approximation methods tailored for specific scenarios.

As discussed in Sec. IV, the common controllability, normality, and strong observability conditions can imply Condition 2 if the control constraint set belongs to Type 2 (with Type 1 as a special case of Type 2). Therefore, it is desirable for the control constraint set to belong to Type 2. The following theorem offers a suitable approximation method for a control constraint set that does not belong to Type 2.

THEOREM 5 ([29]) *For any control constraint set $\mathcal{U}$ not belonging to Type 2 and for every $\epsilon > 0$, there exists a Type 2 approximating set $\mathcal{U}_\epsilon$ such that $d_H(\mathcal{U},\mathcal{U}_\epsilon) < \epsilon$ where $d_H(\cdot,\cdot)$ is the Hausdorff distance*[3].

Based on Theorem 5, we can approximate any control constraint set that does not belong to Type 2 into a Type 2 set, with the approximation error made arbitrarily small.

For the OP with the control constraint set of Type 2, the controllability, normality, and strong observability conditions can be utilized to check Condition 2. However, apart from normality, it is still challenging to approximate a system that does not meet these conditions into one that does. We address the normality condition specifically through the following result

THEOREM 6 *Given the system (A, B) and the pair (a, b) in the cost function, for any $\epsilon > 0$, there exists an approximate (A_ϵ, B_ϵ) and (a_ϵ, b_ϵ) such that the corresponding $(\hat{A}_\epsilon, \hat{B}_\epsilon, \mathcal{W})$ is normal [see Eq. (12) for the definition of $(\hat{A}_\epsilon, \hat{B}_\epsilon)$], with $\|\hat{A}(t) - \hat{A}_\epsilon(t)\|_{L^\infty} < \epsilon$ and $\|\hat{B}(t) - \hat{B}_\epsilon(t)\|_{L^\infty} < \epsilon$.*

Proof:
The proof is almost the same as Proposition 2 of [28] which considers the case $b(t) = 0$. ■

If the optimal solution of the RP makes $x^*(t) \in \mathrm{bd}\mathcal{X}$ on a discrete set of t, then we only need to consider the subintervals $[t_1, t_2]$ where $x^*(t) \in \mathrm{int}\mathcal{X}$ for verifying Condition 2. Therefore, Theorem 5-6 ensure that any OP can be approximated to satisfy Condition 2 with the approximation error being made arbitrarily small.

VI. Application Example

This section presents a Mars landing case study to validate the proposed theoretical framework. While prior work [1], [2], [28], [35] has established exact convex relaxation methods for scenarios with the glide-slope constraint inactive or only active on a point, our results extend these capabilities to more complex cases where the glide-slope constraint may remain active over continuous time intervals.

[3]The Hausdorff distance of two compact sets X and Y is defined by $d_H(X,Y) = \max\{\max_{a\in X} d(a,Y), \max_{b\in Y} d(b,X)\}$.

A. Problem Formulation and Transformation

The fuel-optimal Mars landing problem is formulated as [1], [2], [28]

$$\begin{aligned}\min \quad & \int_{t_0}^{t_f} \|u(t)\| \mathrm{d}t \\ \text{s.t.} \quad & \dot{x}(t) = Ax(t) + B\frac{u(t)}{m(t)} + c \\ & \dot{m}(t) = -\|u(t)\|/v_{\text{ex}} \\ & \rho_1 \le \|u(t)\| \le \rho_2,\ u_1(t) \ge \|u(t)\| \cos\theta_{\max} \\ & \|x_{2:3}(t)\| \le x_1(t)/\tan\gamma_{\min} \\ & x(t_0) = x_0,\ m(t_0) = m_0,\ x(t_f) = 0\end{aligned} \tag{39}$$

The state vector $x(t) = [r(t)^\top\ \dot{r}(t)^\top]^\top$ represents position and velocity, with $r(t) = [r_1(t)\ \ r_2(t)\ \ r_3(t)]^\top \in \mathbb{R}^3$ denoting the 3-D position (where $r_1(t)$ is the altitude). The control input $u(t) \in \mathbb{R}^3$ is the thrust vector subject to magnitude constraints between ρ_1 and ρ_2, and a maximum tilt angle $\theta_{\max}$ defined through $\theta := \cos^{-1}(u_1/\|u\|)$. The glide slope constraint ensures the vehicle maintains a minimum approach angle $\gamma_{\min}$, defined as $\gamma := \tan^{-1}(x_3/\|x_{1:2}\|)$. The mass of the vehicle is denoted by $m(t)$, which decreases over time due to fuel consumption with an exhaust velocity v_{ex}. The system dynamics are governed by the matrices A and B defined as [2]

$$A = \begin{bmatrix} 0 & I_3 \\ -S(\omega)^2 & -2S(\omega) \end{bmatrix},\ B = \begin{bmatrix} 0 \\ I_3 \end{bmatrix} \tag{40}$$

where $\omega \in \mathbb{R}^3$ represents the Mars angular velocity and $S(\omega)$ is the corresponding skew-symmetric matrix as follows

$$S(\omega) = \begin{bmatrix} 0 & -\omega_3 & \omega_2 \\ \omega_3 & 0 & -\omega_1 \\ -\omega_2 & \omega_1 & 0 \end{bmatrix} \tag{41}$$

The vector c is defined as $c = [0\ 0\ 0\ \ -g_0\ 0\ 0]^\top$ where g_0 is the constant gravitational acceleration.

While the original fuel-optimal problem (39) falls outside the scope of the general optimal control problem considered in this paper [see the form of the OP in Eq. (1)], we employ the relaxation technique developed in [28] to transform it. The relaxed formulation introduces a slack variable $\sigma(t) \in \mathbb{R}$, yielding the following problem

$$\begin{aligned}\min \quad & \int_{t_0}^{t_f} \sigma(t) \mathrm{d}t \\ \text{s.t.} \quad & \dot{x}(t) = Ax(t) + B\frac{u(t)}{m(t)} + c \\ & \dot{m}(t) = -\sigma(t)/v_{\text{ex}} \\ & \|u(t)\| \le \sigma(t) \\ & \rho_1 \le \sigma(t) \le \rho_2,\ u_1(t) \ge \sigma(t)\cos\theta_{\max} \\ & \|x_{2:3}(t)\| \le x_1(t)/\tan\gamma_{\min} \\ & x(t_0) = x_0,\ m(t_0) = m_0,\ x(t_f) = 0\end{aligned} \tag{42}$$

This problem can easily be solved by transforming it into a convex problem (see Appendix of [28]). We use σ^* and m^* to denote the optimal σ and m of the problem (42), respectively.

The relationship between the original fuel-optimal problem (39) and its relaxed version (42) can be understood through the following analysis. While any optimal solution of the original problem naturally provides a feasible solution to the relaxed problem, the converse requires the additional condition that the relaxed solution must satisfy the constraint $\|u(t)\| = \sigma(t)$. Building upon the theoretical framework established in [28], we recognize that when a solution pair (x, u) is found such that (x, u, m^*, σ^*) satisfies the dynamics, the constraint $\|u(t)\| = \sigma^*(t)$, and all other constraints in the relaxed problem (42), (x, m^*, u) necessarily constitutes an optimal solution to the original problem (39). This insight motivates the construction of the following auxiliary problem, which is designed to explicitly enforce the critical thrust magnitude constraint through appropriate variable transformations.

$$\begin{aligned}\min \quad & \int_{t_0}^{t_f} a^\top x(t) \mathrm{d}t \\ \text{s.t.} \quad & \dot{x}(t) = Ax(t) + \tilde{B}(t)\tilde{u}(t) + c \\ & \|\tilde{u}(t)\| = 1,\ \tilde{u}_1(t) \ge \cos\theta_{\max} \\ & \|x_{2:3}(t)\| \le x_1(t)/\tan\gamma_{\min} \\ & x(t_0) = x_0,\ x(t_f) = 0\end{aligned} \tag{43}$$

where $a \in \mathbb{R}^6$ is nonzero, $\tilde{u}(t) = u(t)/\sigma^*(t)$, and $\tilde{B}(t) = B\sigma^*(t)/m^*(t)$. The problem maintains the standard OP structure. Let $(x^*, \tilde{u}^*)$ denote the optimal solution of the problem (43). Through the inverse transformation $u^* := \sigma^*\tilde{u}^*$, we obtain a control profile that inherently satisfies the thrust magnitude constraint $\|u^*(t)\| = \sigma^*(t)$ by construction. Thus, the transformed solution (x^*, m^*, u^*) is the optimal solution of the original problem (39).

REMARK 6 *While any nonzero a is theoretically sufficient to satisfy Condition 1, its practical significance lies in its direct influence on the system matrix $\hat{A}$ which is crucial for verifying Condition 2. Although no formal systematic procedure for selecting a exists, its choice is guided by the need to satisfy Condition 2.*

Next, we will apply the theoretical results of this paper to the problem (43), and obtain an optimal solution of the original problem (39).

B. Numerical Results

For the problem (43), Condition 1 is automatically satisfied as the cost functional is a nonzero integral. Consequently, the exactness of the convex relaxation depends solely on verifying Condition 2. Our verification considers two distinct scenarios:

Discrete activeness case: When the glide-slope constraint is active only at isolated points, we establish Condition 2 by examining the system's normality.

Continuous activeness case: When the glide-slope constraint is active over continuous subintervals, we verify Condition 2 by checking the controllability and strong observability of the system. In this case, we remove

the constraint $\tilde{u}_1(t) \geq \cos\theta_{\max}$ to satisfy Condition 2. It is important to note that if the glide-slope constraint is active over continuous subintervals and the constraint $\tilde{u}_1(t) \geq \cos\theta_{\max}$ is retained, Condition 2 will not hold.

The parameters used for numerical computation can be seen in Table I. The RP corresponding to the problem (43) will be discretized by Euler method with 51 uniform nodes, resulting in a second-order cone programming (SOCP) problem. The SOCP is solved using the MOSEK solver [19] on a laptop with an Intel Core Ultra 9 285H 2.90 GHz CPU.

TABLE I

The parameters used for numerical computation.

Parameter	Value	Unit
a	$[0\ 0\ 1\ 0\ 0\ 0]^\top$	-
ω	$[2.53\times10^{-5}\ 0\ 6.62\times10^{-5}]^\top$	rad/s
g_0	3.7114	m/s^2
v_{ex}	2549.8	m/s
ρ_1	13	kN
ρ_2	19	kN
$\theta_{\max}$	45	deg
$\gamma_{\min}$	30	deg
m_0	2110	kg
t_0	0	s
t_f	72	s

1. *Discrete activeness case*

We first examine the case where the glide-slope constraint activates only at discrete time points. The initial position and velocity are set as Table II. The control constraint set is $\mathcal{U} = \{\tilde{u} : \|\tilde{u}\| = 1,\ \tilde{u}_1 \geq \cos\theta_{\max}\}$, and its convex hull is $\text{co}\mathcal{U} = \{\tilde{u} : \|\tilde{u}\| \leq 1,\ \tilde{u}_1 \geq \cos\theta_{\max}\}$. The set difference $\text{co}\mathcal{U} \setminus \mathcal{U}$ decomposes into two distinct relative interiors:

$$\begin{aligned} \text{ri}\mathcal{M}_1 =& \text{int}(\text{co}\mathcal{U}) \\ \text{ri}\mathcal{M}_2 =& \{\tilde{u} : \|\tilde{u}\| < 1,\ \tilde{u}_1 = \cos\theta_{\max}\} \end{aligned} \tag{44}$$

This structure classifies $\mathcal{U}$ as Type 2. The corresponding test vector set is constructed as $\mathcal{W} = \{[0\ 1\ 0]^\top\}$, chosen to verify the normality.

TABLE II

The initial position and velocity for the discrete activeness case.

Parameter	Value	Unit
r_0	$[4\ \ -2.5\ 1.8]^\top$	km
$\dot{r}_0$	$[-90\ \ -30\ 45]^\top$	m/s

The sufficient conditions for exact convex relaxation are verified as follows. Condition 1 is satisfied since the cost functional is a nonzero integral. For Condition 2, the discrete activeness of glide-slope constraints implies verification reduces to checking system normality according to Theorem 3. The original $(\hat{A}, \hat{B}, \mathcal{W})$ fails to meet the normality. Therefore, based on Theorem 6, we approximate the matrix $\hat{A}$ into $\hat{A}_\epsilon$ by introducing a small perturbation $\epsilon = 1\times10^{-5}$ to the (42)-th entry of the matrix $\hat{A}$ while preserving all other entries. This yields a perturbed system $(\hat{A}, \hat{B}, \mathcal{W})$ that satisfies the normality condition.

It takes about 30 ms to get the optimal solution by solving the problem (42) and the relaxed version of the problem (43) in sequence. The numerical results demonstrate successful implementation of the proposed convex relaxation approach. The blue solid line of Fig. 1 presents the three-dimensional trajectory, revealing that the glide-slope constraint becomes active at only one discrete point, as further corroborated by the blue solid line of Fig. 2(a). The blue solid line of Fig. 2(b) displays the tilt angle profile, showing full compliance with the prescribed maximum tilt angle. Most critically, Fig. 2(c) confirms that the relaxed thrust magnitude constraint $\|\tilde{u}(t)\| \leq 1$ (equivalent to $\|u(t)\| \leq \sigma^*(t)$) remains active for the entire time horizon, with the optimal solution consistently achieving equality. Therefore, the exact convex relaxation is achieved which is consistent with Theorem 1.

To rigorously evaluate the accuracy of the approximation, we compared the solution against a benchmark obtained by solving the problem (43) directly via the nonlinear optimization solver IPOPT [18]. The true solution (the red dashed lines in Figs. 1 and 2) almost coincides with the solution obtained by our method. This confirms that the error introduced by the approximation of matrix $\hat{A}$ is negligible.

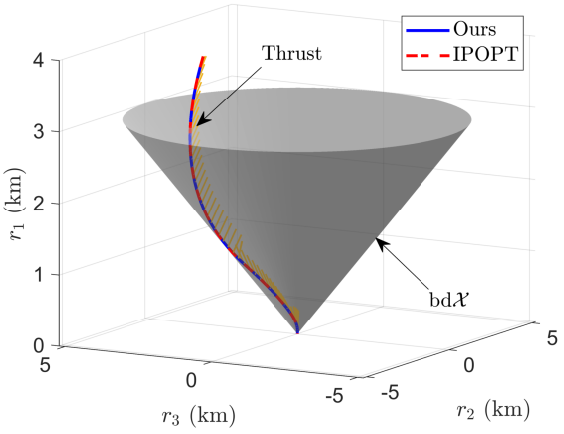

Fig. 1. The 3-D trajectory, the thrust dirction, and the boundary of the glide-slope constraint for the discrete activeness case.

2. *Continuous activeness case*

We now examine the case where the glide-slope constraint remains active over continuous time subintervals. The initial position and velocity are set as Table III. In this mission, we remove the tilt constraint $\tilde{u}_1(t) \geq \cos\theta_{\max}$ for the satisfaction of Condition 2. Thus, the control constraint set is $\mathcal{U} = \{\tilde{u} : \|\tilde{u}\| = 1\}$, and its convex hull is $\text{co}\mathcal{U} = \{\tilde{u} : \|\tilde{u}\| \leq 1\}$. The set $\mathcal{U}$ belongs to Type 1 because $\text{bd}(\text{co}\mathcal{U}) \subset \mathcal{U}$. It is worth noting that simplifying the problem by omitting the tilt constraint is a common approach in the literature on Mars landing guidance [1],

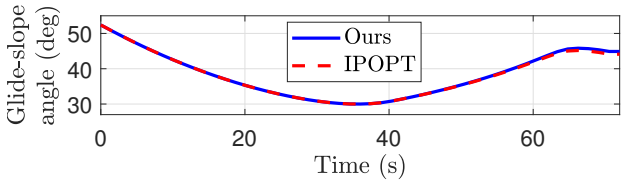

(a) The glide-slope angle profile.

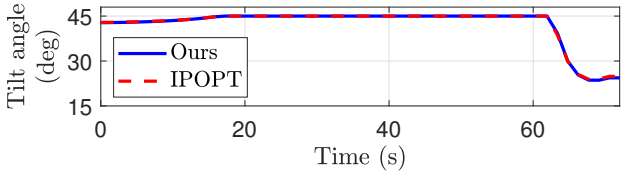

(b) The tilt angle profile.

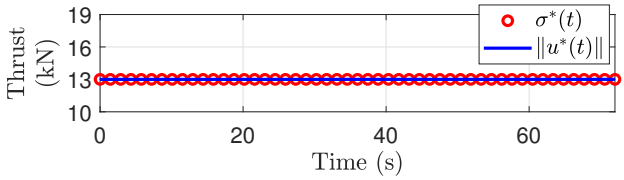

(c) The status of the relaxed constraint $\|\tilde{u}(t)\| \leq 1$.

Fig. 2. The glide-slope angle profile, the tilt angle profile, and the status of the relaxed constraint $\|\tilde{u}(t)\| \leq 1$ for the discrete activeness case.

[35], [43], [44], which allows for a focused analysis on other complex aspects of the problem.

TABLE III
The initial position and velocity for the continuous activeness case.

Parameter	Value	Unit
r_0	$[5.2 \ -2.5 \ -2]^\top$	km
$\dot{r}_0$	$[-120 \ -50 \ 0]^\top$	m/s

In addition, we approximate the glide-slope constraint into a linear constraint in order to apply the results in Sec. IV to verify Condition 2. The original glide-slope constraint $\{x : \|x_{2:3}\| \leq x_1/\tan\gamma_{\min}\}$ is a second-order cone constraint, which is shown in the left plot of Fig. 3. We approximate it into linear constraints, which is illustrated as a pyramid in the right plot of Fig. 3. The pyramid is composed of 30 planes, and each normal vector of the planes can be expressed as

$$\hat{n}_i = [-\cos\gamma_{\min} \ \ -\sin\gamma_{\min}\cos\beta_i \ \ -\sin\gamma_{\min}\sin\beta_i]^\top \tag{45}$$

where $\beta_i = 2\pi i/30$ for $i = 1, \ldots, 30$. Therefore, the approximated linear glide-slope constraint can be expressed as $\{x : Gx \leq 0\}$ where

$$G = \begin{bmatrix} \hat{n}_1^\top & 0 \\ \vdots & \vdots \\ \hat{n}_{30}^\top & 0 \end{bmatrix} \tag{46}$$

We proceed to verify whether the sufficient conditions for optimality are satisfied in our problem formulation. First, we observe that Condition 1 is clearly satisfied by construction. Regarding Condition 2, since we allow

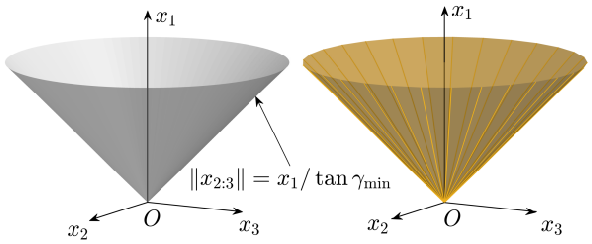

Fig. 3. The original glide-slope constraint set (left) and the approximated linear glide-slope constraint set (right).

the glide-slope constraint to be active on arbitrary subintervals, it follows from Theorem 2 that we can verify Condition 2 by checking the controllability of $(\hat{A}, \hat{B})$ and the strong observability of $(-\hat{A}^\top, \hat{D}_j, \hat{B}^\top, 0)$ for each $j = 1, \ldots, 60$, where $\hat{D}_j = [D_j \ 0]^\top$ and

$$D_j = \begin{cases} [\hat{n}_j^\top \ 0] & j = 1, \ldots, 30 \\ \begin{bmatrix} \hat{n}_{j-30}^\top & 0 \\ \hat{n}_{j-29}^\top & 0 \end{bmatrix} & j = 31, \ldots, 59 \\ \begin{bmatrix} \hat{n}_1^\top & 0 \\ \hat{n}_{30}^\top & 0 \end{bmatrix} & j = 60 \end{cases} \tag{47}$$

It can be seen that the system $(\hat{A}, \hat{B})$ is controllable and the system $(-\hat{A}^\top, \hat{D}_j, \hat{B}^\top, 0)$ is strongly observable for each $j = 1, \ldots, 60$ (see Theorem 7 for the approach to check strong observability). Therefore, Condition 2 is satisfied.

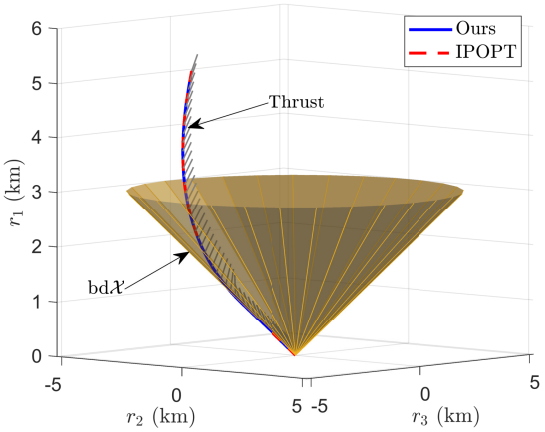

Fig. 4. The 3-D trajectory, the thrust dirction, and the boundary of the glide-slope constraint for the continuous activeness case.

It takes about 30 ms to get the optimal solution by solving the problem (42) and the relaxed version of the problem (43) in sequence. The results are illustrated in Figs. 4 and 5. The blue solid line of Fig. 4 presents the 3-D trajectory of the lander, which in conjunction with the blue solid line of Fig. 5(a), clearly shows the activeness of the glide-slope constraint over a continuous subinterval. The tilt angle θ is shown in the blue solid line of Fig. 5(b). Most significantly, Fig. 5(c) demonstrates that the thrust magnitude constraint $\|\tilde{u}(t)\| \leq 1$ (equivalent to

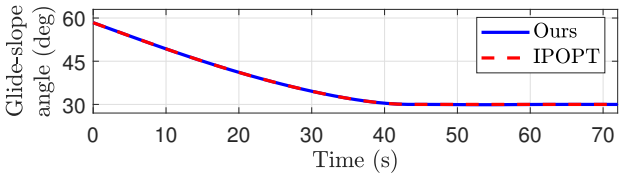

(a) The glide-slope angle profile.

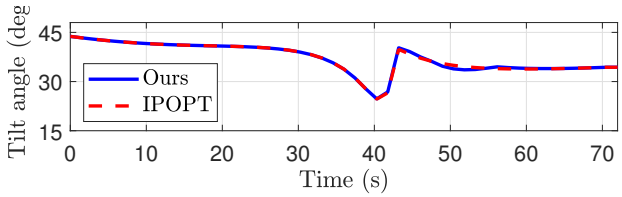

(b) The tilt angle profile.

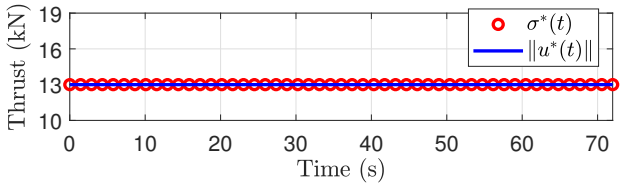

(c) The status of the relaxed constraint $\|\tilde{u}(t)\| \leq 1$.

Fig. 5. The glide-slope angle profile, the tilt angle profile, and the status of the relaxed constraint $\|\tilde{u}(t)\| \leq 1$ for the continuous activeness case.

$\|u(t)\| \leq \sigma^*(t)$) remains active for the entire duration of the trajectory. This implies that the exact convex relaxation is achieved which is consistent with Theorem 1.

To rigorously evaluate the accuracy of the approximation of the glide-slope constraint, we compared the solution obtained by our method against a benchmark solution obtained by solving the problem (43) directly via the IPOPT [18]. The true solution (the red dashed lines in Figs. 4 and 5) also almost coincides with our solution. This validates that the error introduced by the approximation of the glide-slope constraint is negligible.

VII. Conclusion

This paper addresses the challenge of achieving exact convex relaxation for general nonconvex OCPs. Two unified sufficient conditions—Condition 1 and 2—are proposed to ensure the exactness of the relaxation, and a novel proof technique based on a locally constructed subproblem is introduced. For control and state constraint sets of some specific forms, we show how one of the proposed sufficient conditions can be transformed into the classical controllability, normality, and strong observability conditions. Additionally, we provide approximation methods to ensure that these sufficient conditions are met in some specific scenarios. The numerical example of the Mars landing problem confirms our theoretical results, demonstrating that nonconvex problems can be converted into convex problems using the proposed sufficient conditions.

APPENDIX

Consider the linear time-varying system on a time interval I as follows

$$\begin{aligned} \dot{x}(t) &= A(t)x(t) + B(t)u(t) \\ y(t) &= C(t)x(t) + D(t)u(t) \end{aligned} \tag{48}$$

where $x(t) \in \mathbb{R}^n$, $u(t) \in \mathbb{R}^m$, and $y(t) \in \mathbb{R}^p$ denotes the state, the control input, and the output, respectively. The coefficient matrices A, B, C, and D are assumed to be smooth. The definition of strong observability is given as follows.

DEFINITION 2 ([26], [45]) *The system (A, B, C, D) is strongly observable if zero output $y(t) \equiv 0$ implies zero state $x(t) \equiv 0$ for any input $u(t)$.*

Next, we introduce a method to check the strong observability of the system (A, B, C, D). First, we define the matrices Q and T as follows [45]

$$Q(t) = [C_0^\top \ \cdots \ C_{n-1}^\top]^\top \tag{49}$$

$$T(t) = \begin{bmatrix} T_{0,0}(t) & 0 & \cdots & 0 \\ T_{1,0}(t) & T_{1,1}(t) & \cdots & 0 \\ \vdots & \vdots & \ddots & \vdots \\ T_{n-1,0}(t) & T_{n-1,1}(t) & \cdots & T_{n-1,n-1}(t) \end{bmatrix} \tag{50}$$

where

$$C_0(t) = C(t) \tag{51}$$

$$C_i(t) = C_{i-1}(t)A(t) + \dot{C}_{i-1}(t), \ i = 1, \ldots, n-1 \tag{52}$$

$$T_{i,i}(t) = D(t), \ 0 \leq i \leq n-1 \tag{53}$$

$$T_{i,0}(t) = C_{i-1}(t)B(t) + \dot{T}_{i-1,0}(t), \ 1 \leq i \leq n-1 \tag{54}$$

$$T_{i,j}(t) = T_{i-1,j-1}(t) + \dot{T}_{i-1,j}(t), \ 1 \leq j < i \leq n-1 \tag{55}$$

With the matrices Q and T, we can check the strong observability by the following theorem.

THEOREM 7 ([45]) *The system (A, B, C, D) is strongly observable if and only if*

$$\operatorname{rank}[Q(t) \ T(t)] - \operatorname{rank} T(t) = n, \ \forall t \in I \setminus E \tag{56}$$

where E is a nowhere dense set of I.

REFERENCES

[1] B. Açıkmeşe and S. R. Ploen
Convex programming approach to powered descent guidance for mars landing
Journal of Guidance, Control, and Dynamics, vol. 30, no. 5, pp. 1353–1366, 2007.

[2] B. Açıkmeşe, J. M. Carson, and L. Blackmore
Lossless convexification of nonconvex control bound and pointing constraints of the soft landing optimal control problem
IEEE Transactions on Control Systems Technology, vol. 21, no. 6, pp. 2104–2113, 2013.

[3] P. Lu and X. Liu
Autonomous trajectory planning for rendezvous and proximity operations by conic optimization
Journal of Guidance, Control, and Dynamics, vol. 36, no. 2, pp. 375–389, 2013.

[4] M. Szmuk, B. Acikmese, and A. W. Berning
Successive convexification for fuel-optimal powered landing with aerodynamic drag and non-convex constraints
In *AIAA Guidance, Navigation, and Control Conference*. AIAA 2016-0378, 2016.

[5] R. Yang and X. Liu
Fuel-optimal powered descent guidance with free final-time and path constraints
Acta Astronautica, vol. 172, pp. 70–81, 2020.

[6] M. Szmuk, C. A. Pascucci, and B. Açıkmeşe
Real-time quad-rotor path planning for mobile obstacle avoidance using convex optimization
In *2018 IEEE/RSJ International Conference on Intelligent Robots and Systems (IROS)*. IEEE, 2018, pp. 5906–5911.

[7] P. Zarchan
Tactical and strategic missile guidance, sixth edition. American Institute of Aeronautics and Astronautics, Inc., 2012.

[8] A. R. Klumpp
Apollo lunar descent guidance
Automatica, vol. 10, no. 2, pp. 133–146, 1974.

[9] S. J. Citron, S. E. Dunin, and H. F. Meissinger
A terminal guidance technique for lunar landing
AIAA Journal, vol. 2, no. 3, pp. 503–509, 1964.

[10] D. C. Chandler and I. E. Smith
Development of the iterative guidance mode with its application to various vehicles and missions. *Journal of Spacecraft and Rockets*, vol. 4, no. 7, pp. 898–903, 1967.

[11] P. Lu
Introducing computational guidance and control
Journal of Guidance, Control, and Dynamics, vol. 40, no. 2, pp. 193–193, 2017.

[12] B. Açıkmeşe and L. Blackmore
Lossless convexification of a class of optimal control problems with non-convex control constraints
Automatica, vol. 47, no. 2, pp. 341–347, 2011.

[13] X. Liu, Z. Shen, and P. Lu
Entry trajectory optimization by second-order cone programming
Journal of Guidance, Control, and Dynamics, vol. 39, no. 2, pp. 227–241, 2016.

[14] X. Liu, Z. Shen, and P. Lu
Exact convex relaxation for optimal flight of aerodynamically controlled missiles
IEEE Transactions on Aerospace and Electronic Systems, vol. 52, no. 4, pp. 1881–1892, 2016.

[15] X. Liu
Convergence-guaranteed trajectory planning for a class of nonlinear systems with nonconvex state constraints
IEEE Transactions on Aerospace and Electronic Systems, vol. 58, no. 3, pp. 2243–2256, 2022.

[16] C. Büskens and H. Maurer
SQP-methods for solving optimal control problems with control and state constraints: adjoint variables, sensitivity analysis and real-time control
Journal of Computational and Applied Mathematics, vol. 120, no. 1-2, pp. 85–108, 2000.

[17] P. E. Gill, W. Murray, and M. A. Saunders
SNOPT: An SQP algorithm for large-scale constrained optimization
SIAM Review, vol. 47, no. 1, pp. 99–131, 2005.

[18] L. T. Biegler and V. M. Zavala
Large-scale nonlinear programming using IPOPT: An integrating framework for enterprise-wide dynamic optimization
Computers & Chemical Engineering, vol. 33, no. 3, pp. 575–582, 2009.

[19] E. D. Andersen, C. Roos, and T. Terlaky
On implementing a primal-dual interior-point method for conic quadratic optimization
Mathematical Programming, vol. 95, no. 2, pp. 249–277, 2003.

[20] A. Domahidi, E. Chu, and S. Boyd
ECOS: An SOCP solver for embedded systems
In *2013 European Control Conference (ECC)*. IEEE, 2013, pp. 3071–3076.

[21] L. Blackmore, B. Açıkmeşe, and J. M. Carson
Lossless convexification of control constraints for a class of nonlinear optimal control problems
Systems & Control Letters, vol. 61, no. 8, pp. 863–870, 2012.

[22] M. W. Harris and B. Açıkmeşe
Lossless convexification of non-convex optimal control problems for state constrained linear systems
Automatica, vol. 50, no. 9, pp. 2304–2311, 2014.

[23] D. Malyuta and B. Açıkmeşe
Lossless convexification of optimal control problems with semi-continuous inputs
IFAC-PapersOnLine, vol. 53, no. 2, pp. 6843–6850, 2020.

[24] S. Kunhippurayil, M. W. Harris, and O. Jansson
Lossless convexification of optimal control problems with annular control constraints
Automatica, vol. 133, p. 109848, 2021.

[25] M. W. Harris
Optimal control on disconnected sets using extreme point relaxations and normality approximations
IEEE Transactions on Automatic Control, vol. 66, no. 12, pp. 6063–6070, 2021.

[26] N. T. Woodford and M. W. Harris
Geometric properties of time-optimal controls with state constraints using strong observability
IEEE Transactions on Automatic Control, vol. 67, no. 12, pp. 6881–6887, 2022.

[27] D. Malyuta *et al.*
Convex optimization for trajectory generation: A tutorial on generating dynamically feasible trajectories reliably and efficiently
IEEE Control Systems, vol. 42, no. 5, pp. 40–113, 2022.

[28] R. Yang, X. Liu, and D. Lin
Exact relaxation of nonconvex optimal control problems based on problem reconstruction
Journal of Guidance, Control, and Dynamics, vol. 47, no. 4, pp. 761–769, 2024.

[29] R. Yang and X. Liu
Convex hull relaxation of optimal control problems with general nonconvex control constraints
IEEE Transactions on Automatic Control, vol. 69, no. 6, pp. 4028–4034, 2024.

[30] Y. Guo, Q. Liu, and X. He
Active fault diagnosis for stochastic systems subject to non-convex input constraints
Automatica, vol. 164, p. 111631, 2024.

[31] L. S. Pontryagin, V. G. Boltyanskii, R. V. Gamkrelidze, and E. F. Mishchenko
The mathematical theory of optimal processes. CRC Press, 1986.

[32] L. D. Berkovitz and N. G. Medhin
Nonlinear optimal control theory. CRC Press, 2012.

[33] H. Frankowska
Regularity of minimizers and of adjoint states in optimal control under state constraints
Journal of Convex Analysis, vol. 13, no. 2, pp. 299–328, 2006.

[34] H. Frankowska
Optimal control under state constraints
In *Proceedings of the International Congress of Mathematicians 2010 (ICM 2010)*, 2011, pp. 2915–2942.

[35] L. Blackmore, B. Açıkmeşe, and D. P. Scharf
Minimum-landing-error powered-descent guidance for mars landing using convex optimization
Journal of Guidance, Control, and Dynamics, vol. 33, no. 4, pp. 1161–1171, 2010.

[36] R. F. Hartl, S. P. Sethi, and R. G. Vickson
A survey of the maximum principles for optimal control problems with state constraints
SIAM Review, vol. 37, no. 2, pp. 181–218, 1995.

[37] R. T. Rockafellar
Convex analysis. Princeton University Press, 1972.
[38] A. A. Milyutin
On a certain family of optimal control problems with phase constraint
Journal of Mathematical Sciences, vol. 100, no. 5, pp. 2564–2571, 2000.
[39] H. Federer
Curvature measures
Transactions of the American Mathematical Society, vol. 93, no. 3, pp. 418–491, 1959.
[40] R. Schneider
Polyhedral approximation of smooth convex bodies
Journal of Mathematical Analysis and Applications, vol. 128, no. 2, pp. 470–474, 1987.
[41] D. Dörfler
On the approximation of unbounded convex sets by polyhedra
Journal of Optimization Theory and Applications, vol. 194, no. 1, pp. 265–287, 2022.
[42] E. B. Lee and L. Markus
Foundations of optimal control theory. John Wiley, 1967.
[43] M. W. Harris and B. Açıkmeşe
Maximum divert for planetary landing using convex optimization
Journal of Optimization Theory and Applications, vol. 162, no. 3, pp. 975–995, 2013.
[44] S. You, R. Dai, and J. R. Rea
Theoretical analysis of fuel-optimal powered descent problem with state constraints
Journal of Guidance, Control, and Dynamics, vol. 45, no. 12, pp. 2350–2359, 2022.
[45] N. T. Woodford and M. W. Harris
Strong observability of ltv systems with feedthrough and on-orbit reconnaissance and evasion applications
IEEE Control Systems Letters, vol. 7, pp. 811–816, 2023.

Runqiu Yang (Member, IEEE) received the BSc degree in flight vehicle design and engineering from Beijing Institute of Technology, Beijing, China, in 2018, and the PhD degree in aeronautical and astronautical science and technology from Beijing Institute of Technology, Beijing, China, in 2024. He is currently a postdoctoral fellow with the Department of Aeronautical and Aviation Engineering, The Hong Kong Polytechnic University, Hong Kong, China. His research interests include convex optimization, optimal control, model predictive control, reinforcement learning, and their applications in aerospace engineering and robotics.

Weisong Wen (Member, IEEE) received the B.Eng. degree in mechanical engineering from Beijing Information Science and Technology University (BISTU), Beijing, China, in 2015, the M.Eng. degree in mechanical engineering from China Agricultural University in 2017, and the Ph.D. degree in mechanical engineering from The Hong Kong Polytechnic University (PolyU) in 2020. He was a Visiting Ph.D. Student with the Faculty of Engineering, University of California at Berkeley (UC Berkeley), in 2018. Before joining PolyU as an Assistant Professor in 2023, he has been a Research Assistant Professor with AAE, PolyU, since 2021. He has published 30 SCI articles and 40 conference papers in the field of GNSS (ION GNSS+) and navigation for robotic systems (IEEE ICRA and IEEE ITSC), such as autonomous driving vehicles. He won the Innovation Award from TechConnect 2021, the Best Presentation Award from the Institute of Navigation (ION) in 2020, and the First Prize in Hong Kong Section in Qianhai–Guangdong–Macao Youth Innovation and Entrepreneurship Competition in 2019, based on his research achievements in 3D LiDAR aided GNSS positioning for robotics navigation in urban canyons. The developed 3D LiDAR-aided GNSS positioning method has been reported by top magazines such as Inside GNSS and has attracted industry recognition with remarkable knowledge transfer.

Peiwen Yang received the M.S. degree in the School of Information and Electronics, Beijing Institute of Technology, Beijing, China, in 2019. He is currently a Ph.D. student in the Department of Aeronautical and Aviation Engineering, at the Hong Kong Polytechnic University. His current research interests include aerial vehicle control, computer vision, and robotics.

Zichen Zhao was born in 1997. He received the BSc degree in flight vehicle design and engineering from Beijing Institute of Technology, Beijing, China, in 2019, and the PhD degree in aeronautical and astronautical science and technology from Beijing Institute of Technology, Beijing, China, in 2025. He is currently an associate research fellow at Harbin Institute of Technology, Harbin, China. His main research fields include spacecraft dynamics and control, research on space debris removal systems and technologies, and the application and implementation of artificial intelligence methods in the aerospace field.

Fengtianyi Huang is currently an undergraduate student with the School of Automation, Northwestern Polytechnical University, Xi'an, China. Her main research fields include optimal control and reinforcement learning.